Uncovering the Impact of COVID-19 Mediated Bidirectional Dysregulation of CYP3A4 on Systemic and Pulmonary Drug Concentrations Using Physiologically Based Pharmacokinetic Modeling

Chukwunonso K. Nwabufo[1,2,3,4]*

Present address:

[1]Department of Pharmaceutical Sciences, Leslie Dan Faculty of Pharmacy, University of Toronto, Toronto, ON, Canada;

[2]OneDrug Inc., Toronto, ON, Canada;

Previous address:

[3]Program in Translational Medicine, Hospital for Sick Children, Toronto, ON, Canada;

[4]Centre for Applied Pharmacokinetic Research, School of Health Sciences, University of Manchester, Manchester, UK

Running Title: Impact of COVID-19 on Intercompartmental Drug Concentrations

*Corresponding Author

Name: Chukwunonso K. Nwabufo

Address: Department of Pharmaceutical Sciences

          Leslie Dan Faculty of Pharmacy, University of Toronto

          144 College Street, Toronto, ON, M5S 3M2

Email address: Chukwunonso.nwabufo@mail.utoronto.ca

Number of text pages: 36

Number of tables: 6

Number of figures: 5

Number of references: 42

The number of words in the —

Abstract: 249

Introduction: 750

Discussion: 1493

Nonstandard abbreviations

AUC	Area under the concentration–time curve
AUC_{plasma}	Area under the concentration–time curve in the plasma compartment
BCRP	Breast cancer resistance protein
BID	Twice a day
B/P	Blood-to-plasma ratio
CL_{int}	Intrinsic clearance
$CL_{int,CYP3A4}$	Intrinsic clearance of cytochrome P450 3A4
$CL_{int,CYP3A4Lung}$	Intrinsic clearance of cytochrome P450 3A4 in the lung using lung CYP1A1 as a surrogate
CL_R	Renal clearance
C_{max}	Maximum concentration
$C_{max,fluid}$	Maximum concentration in the fluid compartment of the right lung low lobe
$C_{max,plasma}$	Maximum concentration in the plasma
$C_{max,tissue\ mass}$	Maximum concentration in the tissue mass compartment of the right lung low lobe
COVID-19	Coronavirus disease 2019
CRP	C-reactive protein
CYP	Cytochrome P450
EC	Effective concentration
EC_{50}	50% effective concentration

EC_{90}	90% effective concentration
ELF	Epithelial lining fluid
f_a	Fraction absorbed
$f_{m,CYP3A4}$	Fraction metabolized by CYP3A4
fu_{fluid}	Fraction unbound in the lung fluid compartment
$f_{u,gut}$	Fraction unbound in the gut
fu_{mass}	Fraction unbound in the tissue mass compartment of the right lung low lobe
$f_{u,mic}$	Fraction unbound in an *in vitro* microsomal incubation
f_{up}	Fraction unbound in the plasma
γ	Hill coefficient
HLM	Human liver microsomes
IC_{50}	50% inhibitory concentration
IC_{90}	90% inhibitory concentration
ICU	Intensive care unit
$IndC_{50}$	Inducer concentration supporting half maximal induction
Ind_{max}	Maximal fold induction over vehicle
k_a	First-order absorption rate constant
K_{app}	The concentration of mechanism-based inhibitor that results in achieving the half maximal rate of inactivation
K_i	Concentration of inhibitor associated with half maximal inhibition
k_{in}, k_{out}	First-order rate constants which act upon the masses of drug within the systemic compartment and the single adjusting compartment,

	respectively
k_{inact}	Inactivation rate of enzyme
K_m	Michaelis-Menten constant
Kp	Tissue-plasma partition coefficient
LogP	Log of the octanol-water partition coefficient
MATE1	Multidrug and toxin extrusion protein 1
MIC_{90}	Minimum inhibitory concentration of an antimicrobial agent that inhibits 90% of a given microbial population
MPPLu	Microsomal protein per lung
MW	Molecular weight
OAT	Organic anion transporter
OATP	Organic anion transporting polypeptide
OCT	Organic cation transporter
PBPK	Physiologically based pharmacokinetic
PD	Pharmacodynamic
P-gp	P-glycoprotein
PK	Pharmacokinetic
pKa	Acid dissociation constant
Q12h	Every 12 hours
QD	Once a day
Q_{gut}	Flow rate for overall delivery of drug to the gut
SARS-CoV-2	Severe acute respiratory syndrome coronavirus 2
V_{max}	Maximum metabolic rate

V_{sac} — Volume of single adjusting compartment

V_{ss} — Steady-state volume of distribution

Abstract

Several clinical studies have shown that COVID-19 increases the systemic concentration of drugs in hospitalized COVID-19 patients. However, it is unclear how COVID-19-mediated bidirectional dysregulation of hepatic and pulmonary CYP3A4 impacts drug concentrations, especially in the lung tissue which is most affected by the disease. Herein, PBPK modeling was used to demonstrate the differences in systemic and pulmonary concentrations of four respiratory infectious disease drugs when CYP3A4 is concurrently downregulated in the liver and upregulated in the lung based on existing clinical data on COVID-19 – CYP3A4 interactions at varying severity levels including outpatients, non-ICU, and ICU patients. The study showed that hepatic metabolism is the primary determinant of both systemic and pulmonary drug concentrations despite the concurrent bidirectional dysregulation of liver and lung CYP3A4. ICU patients had the most systemic and pulmonary drug exposure with a percentage increase in AUC_{plasma} of approximately 44%, 56%, 114%, and 196% for clarithromycin, nirmatrelvir, dexamethasone, and itraconazole, respectively, relative to the healthy group. Within the ICU cohort, clarithromycin exhibited its highest exposure in lung tissue mass with a fold change of 1189, while nirmatrelvir and dexamethasone showed their highest exposure in the plasma compartment, with fold changes of about 126 and 5, respectively, compared to the maximum therapeutic concentrations for their target pathogens. Itraconazole was significantly under-exposed in the lung fluid compartment potentially explaining its limited efficacy for the treatment of COVID-19. These findings underscore the importance of optimizing dosing regimens in at risk ICU patients to enhance both efficacy and safety profiles.

7

Significance Statement

This study investigated whether COVID-19-mediated concurrent hepatic downregulation and pulmonary upregulation of CYP3A4 leads to differences in the systemic and pulmonary concentrations of four respiratory medicines. The study demonstrated that intercompartmental differences in drug concentrations were driven by only hepatic CYP3A4 expression. This work suggests that ICU patients with significant COVID-19 – CYP3A4 interactions may be at risk of clinically relevant COVID-19–drug interactions, highlighting the need for optimizing dosing regimens in this patient group to improve safety and efficacy.

Introduction

Understanding the impact of physiological characteristics on pharmacokinetic (PK) and pharmacodynamic (PD) profiles plays an important role in optimizing therapeutic efficacy and safety, both at an individual and subpopulation level. While the influence of pharmacogenotypes on drug PK/PD is widely recognized (Russell *et al.*, 2021), an increasing body of evidence supports the intrinsic effect of pathophysiological pathways on drug PK/PD profiles. For instance, several studies have demonstrated the impact of Coronavirus disease 2019 (COVID-19) on the systemic concentration of drugs. In a clinical investigation, hospitalized COVID-19 patients exhibited a threefold increase in lopinavir plasma trough concentrations, compared to the levels typically seen in HIV-infected patients (Gregoire *et al.*, 2020). Another study revealed a notable increase in tacrolimus serum trough concentration among solid-organ transplant recipients after contracting severe acute respiratory syndrome coronavirus 2 (SARS-CoV-2) infection (Salerno *et al.*, 2021). Additionally, COVID-19 patients admitted to the intensive care unit (ICU) demonstrated increased plasma concentrations of midazolam, which correlated with the inflammatory marker, C-reactive protein (CRP; Le Carpentier *et al.*, 2022). Based on the shared central metabolic pathway, the authors of these three clinical studies suggested that the alterations in systemic drug concentrations could be linked to the repression of the hepatic drug-metabolizing enzyme, CYP3A4, induced by COVID-19-associated inflammatory responses. However, all of these studies have primarily investigated the impact of COVID-19-mediated drug interactions on systemic drug concentrations without considering other peripheral tissues, particularly the lung tissue which is most affected by SARS-CoV-2 infection (Hoffmann *et al.*, 2020; Hou *et al.*, 2020; Ziegler *et al.*, 2020; Rendeiro *et al.*, 2021; Frisoni *et al.*, 2022).

Our group recently reported that the protein expression of CYP3A4 was unaffected in postmortem COVID-19 human lung tissues of 10 patients compared to five age/sex-matched controls (Nwabufo *et al.*, 2023). On the contrary, when our group investigated the changes in *CYP3A4* gene expression in nasopharyngeal swabs from 50 SARS-CoV-2-positive patients (17 outpatients, 16 non-ICU, 17 ICU) and 13 SARS-CoV-2-negative individuals, we observed that *CYP3A4* was upregulated in the non-ICU patient cohort only (Nwabufo *et al.*, 2024). This aligns with our previous study which also demonstrated an upregulation of *CYP3A4* in SARS-CoV-2-infected Vero E6 cells (African monkey kidney epithelial cells; Nwabufo *et al.*, 2023). However, previous clinical studies suggested repression of hepatic CYP3A4 in hospitalized COVID-19 patients (Gregoire *et al.*, 2020; Lenoir *et al.*, 2021; Salerno *et al.*, 2021; Le Carpentier *et al.*, 2022), clearly demonstrating tissue-specific differences in SARS-CoV-2-mediated interactions with CYP3A4.

How this COVID-19-mediated bidirectional dysregulation of hepatic and pulmonary CYP3A4 expression might impact systemic and pulmonary drug concentrations, and by extension intercompartmental differences in safety and efficacy profile is unknown. However, a previous study has shown that under atypical physiological conditions, systemic and peripheral drug concentrations may not be in good agreement. For example, a physiologically based pharmacokinetic (PBPK) modeling study (Rowland Yeo *et al.*, 2020), showed that renal impairment, and a reduction in lung pH from 6.7 to 6 resulted in substantial increases of 30.0-fold, 8.0-fold, and 3.4-fold in lung concentrations of chloroquine, hydroxychloroquine, and azithromycin, respectively. Conversely, systemic drug concentrations experienced only modest increases of approximately 20 to 30% (Rowland Yeo *et al.*, 2020). This suggests potential differences in systemic and pulmonary exposure profiles of the investigated drugs.

10

Under these conditions, personalized medicine can help improve therapeutic efficacy and safety by tailoring treatments to each patient's disease profile and drug processing capacity, thereby addressing potential differences in drug response due to COVID-19-mediated interactions. Understanding the influence of pathophysiology on drug-metabolizing enzymes and their consequential impact on drug concentrations across compartments can help inform therapeutic optimization for affected patient populations. The main objective of this present study is to utilize PBPK modeling and existing clinical data on COVID-19–CYP3A4 interactions to investigate how the simultaneous hepatic downregulation and pulmonary upregulation of CYP3A4, influenced by the severity of COVID-19, impacts systemic and pulmonary drug concentrations in virtual patient cohorts. The drugs investigated in this study are commonly used to treat respiratory infectious diseases, specifically, paxlovid (nirmatrelvir co-packaged with ritonavir), dexamethasone, clarithromycin, and itraconazole, and are primarily metabolized by CYP3A4. By solely incorporating changes in hepatic and pulmonary CYP3A4 expression following COVID-19 severity gradient, while keeping other physiological and pharmacological factors constant in this PBPK modeling study, it becomes possible to clearly identify differences in systemic and pulmonary drug concentrations caused by COVID-19-mediated bidirectional dysregulation of CYP3A4. This highlights the importance of the main organ responsible for metabolizing the investigated drugs and identifies the patient groups most susceptible to safety and efficacy concerns based on drug exposure levels.

Materials and methods

Mechanistic multicompartment lung model development

Simcyp version 22.1 (Simcyp, Sheffield, UK) was used to perform the PBPK modeling of four CYP3A4 substrate drugs including nirmatrelvir coadministered with ritonavir, dexamethasone, clarithromycin, and itraconazole. Activating the permeability-limited lung model in Simcyp was essential to consider lung CYP3A4 metabolism while keeping the lung permeability parameters unchanged as this study did not primarily focus on altering those parameters. The pre-existing mechanistic multicompartment lung model in Simcyp was utilized and has been previously described (Gaohua *et al.*, 2015). The lung consists of seven segments, including upper and lower airways and the lung lobes, specifically, right lung low lobe, right lung middle lobe, right lung top lobe, left lung low lobe, and left lung top lobe (Gaohua *et al.*, 2015). Each segment comprises four compartments representing pulmonary capillary blood, tissue mass (different cell types within the lung tissue), fluid (mucus and epithelial lining fluid, ELF), and alveoli air (Gaohua *et al.*, 2015). The lung model parameters (Supplementary Table S1) and assumptions from Simcyp were used without any modifications (Gaohua *et al.*, 2015).

While changes in drug concentrations across all lung segments were assessed, only drug concentrations within the right lung low lobe were reported because this area is known to be most impacted by COVID-19 (Bösmüller *et al.*, 2021). In the Simcyp lung model, only the CYP1A1 enzyme is pre-defined with limited opportunity of including additional enzymes. To represent CYP3A4 abundance in the lung, CYP1A1 was employed as a surrogate. This implies that each of the investigated drugs had $CL_{int,CYP3A4}$ (representing hepatic CYP3A4 metabolism) and $CL_{int,CYP3A4Lung}$ (representing lung CYP3A4 metabolism using lung CYP1A1 as a surrogate)

12

in the compound elimination section, allowing us to account for both liver and lung CYP3A4 metabolism.

COVID-19 – CYP3A4 interactions data

The lung CYP3A4 abundance level of the healthy cohort was set to 20% (27.4 pmol/mg) of the normal hepatic abundance level of CYP3A4 (137 pmol/mg) as shown in Simcyp version 22.1 (Table 1). This is based on a previous study which revealed that lung activity of CYP3A4 is approximately 20% of its hepatic activity (Anttila *et al.*, 1997). To understand the impact of COVID-19 – CYP3A4 interactions on lung drug concentrations, transcriptomic data on the gene expression of *CYP3A4* in nasopharyngeal swabs from 50 SARS-CoV-2-positive patients (17 outpatients, 16 non-ICU, 17 ICU) and 13 SARS-CoV-2-negative individuals (Table 1) was used to estimate CYP3A4 abundance levels for the respective study cohorts (Nwabufo *et al.*, 2024). This is because recent study from our group uncovered significant expression of drug metabolizing enzymes and membrane transporters in nasopharyngeal samples (Nwabufo *et al.*, 2024), coupled with pre-existing reports of significant metabolic enzyme activity in the nasal cavity (Dahl and Hadley, 1991; Reed, 1993). Furthermore, the nasopharynx is part of the upper airway segment of the lung and is easily accessible, making it an excellent surrogate for lung CYP3A4 expression.

To estimate lung CYP3A4 levels for each COVID-19 patient cohort, the percentage change in nasopharyngeal *CYP3A4* gene expression was multiplied by the lung CYP3A4 abundance in the healthy cohort (Table 1). To estimate hepatic COVID-19 – CYP3A4 interactions, the recently published clinical data that showed % CYP3A4 activity levels in hospitalized COVID-19 patients as a function of midazolam metabolic ratio at different CRP levels (Le Carpentier *et al.*, 2022) was used. To ensure uniformity across the study cohorts, individuals with CRP levels

13

below 50 mg/L were designated as the healthy cohort, reflecting 100% hepatic CYP3A4 activity.

Those with CRP levels between 50 and 150 mg/L were classified as the outpatient COVID-19

cohort, between 150 and 250 mg/L as the non-ICU COVID-19 cohort, and those with CRP levels

exceeding 250 mg/L as the ICU COVID-19 cohort (Table 1). In Simcyp version 22.1, the

standard hepatic CYP3A4 abundance for the healthy cohort was used as a reference. This level

was adjusted for different patient groups: 66% for the outpatient cohort, 53% for the non-ICU

cohort, and 33% for the ICU cohort (Table 1), as previously reported (Le Carpentier *et al.*, 2022).

A consistent coefficient of variation (41%) as reported in Simcyp version 22.1 was applied for

both hepatic and lung CYP3A4 abundance levels across all study cohorts.

<u>Compound parameters and virtual trial information</u>

The input parameters of nirmatrelvir as a component of paxlovid (nirmatrelvir tablets packaged

together with ritonavir tablets) PBPK model were obtained from a recent publication (Sagawa *et al.*, 2023; Table 2). The ritonavir first-order compound file (SV-ritonavir_FO) from the Simcyp

library was used without modifications (Table 2). The Paxlovid PBPK clinical trial involved 12

virtual patients aged 21 to 50 years, with 8.3% being females (Sagawa *et al.*, 2023). The

participants received nirmatrelvir tablets at a dosage of 300 mg twice daily and ritonavir at 100

mg twice daily, both administered for a duration of 5 days (Sagawa *et al.*, 2023; Table 2). The

dexamethasone compound file (SV-dexamethasone) in Simcyp was used (Table 2), and a virtual

population of 100 individuals aged between 18 to 60 years with 50% being females was used for

the simulation as previously reported (Montanha *et al.*, 2022; Table 2). The virtual population

received an oral administration of 6 mg dexamethasone once a day for 10 days (Montanha *et al.*,

2022). The Simcyp clarithromycin compound file (SV-clarithromycin) was modified to a full

PBPK model and V_{ss} was predicted using Kp scaler value of 1.3 to align with clinical study

14

observation (Table 2; Gaohua *et al.*, 2015). Oral administration of 500 mg clarithromycin every 12 hours for a total of 8 doses was simulated in a virtual population comprising 200 individuals aged 20 to 50 years, with a sex distribution of 50% females (Gaohua *et al.*, 2015). The Simcyp itraconazole compound file (SV-Itraconazole_Fasted Soln) was also modified to a full PBPK model and to align with clinical study observations, a Kp scaler value of 0.4393 was employed to achieve a predicted V_{ss} closely resembling the clinical findings (Gaohua *et al.*, 2015; Table 2). The impact of hydroxy-itraconazole metabolite was excluded from the Simcyp model because it inhibits CYP3A4, which could confound the study. To ensure an accurate evaluation of the impact of CYP3A4 dysregulation on itraconazole's PK profile, CYP1A1-mediated metabolism was excluded from consideration. This approach helps isolate the specific role of CYP3A4 without interference from other metabolic pathways. Virtual simulations involved 260 healthy subjects with an age range of 23 to 50 years, including an equal distribution of sex (Gaohua *et al.*, 2015). Itraconazole was given orally at 200 mg twice daily, totaling 10 doses (Gaohua *et al.*, 2015; Table 2).

In vitro effective concentrations values

To demonstrate the relationship between compartmental drug concentrations and effective concentrations (EC) relevant for therapeutic efficacy, reported EC values for the investigated drugs were used (Table 2). While unbound drug concentrations are ideal for comparison with EC values, total drug concentrations are often used as a practical approximation when unbound levels are not readily available, as is the case in this study. The reported EC_{90} value of nirmatrelvir for SARS-CoV-2 variants, specifically omicron ($EC_{90,omicron}$) and delta ($EC_{90,delta}$) was 25 ng/mL (Rosales *et al.*, 2022) and 74.5 ng/mL (European Medicines Agency, 2021; Rosales *et al.*, 2022), respectively. A recent study reported an IC_{50} and IC_{90} of 1.25 ng/mL and

11.20 ng/mL, respectively, for dexamethasone in the context of COVID-19 (Pilla Reddy *et al.*, 2021). The reported minimum inhibitory concentration (MIC_{90}) of clarithromycin for the respiratory pathogen, *Streptococcus pneumoniae* (100 strains; $MIC_{90,S.pneumoniae}$) is 15 ng/mL (Hardy *et al.*, 1992). At least 2 studies have reported *in vitro* EC values of itraconazole for SARS-CoV-2 virus. One study reported an EC_{50} of 1623 ng/mL for itraconazole in Caco-2 cells infected with clinical isolates of SARS-CoV-2 variants – strains, hCoV-19/Germany/FrankfurtFFM1/2020 and BetaCov/Belgium/GHB-03021/2020 (Van Damme *et al.*, 2021). Another research study observed that when Calu-3 and Vero E6 cells were infected with a strain of SARS-CoV-2 known as hCoV-19/Germany/FI1103201/2020, which contains the D614G mutation in the spike protein, they exhibited an $EC_{50,hCoV-19/Germany/FI1103201/2020}$ of 303.41 ng/mL and 275.20 ng/mL, and an $EC_{90,hCoV-19/Germany/FI1103201/2020}$ of 1735.78 ng/mL and 613.87 ng/mL, respectively (Schloer *et al.*, 2021). The EC_{50} and EC_{90} values obtained from the Vero E6 cell study was used. This decision was made because Vero E6 cells have been widely employed in SARS-CoV-2 research, given their significant expression of angiotensin-converting enzyme 2 receptors, which are crucial for the virus's cellular entry (Kumar *et al.*, 2021).

<u>Model verification</u>

The PBPK model was verified by comparing the simulated PK results with the observed clinical PK data for the four investigated drugs. This was done by overlaying the concentration-time profile plots and comparing PK parameters, specifically the C_{max} and AUC values, between the predicted and observed data. To ensure alignment with clinical trials, all simulations were performed using the same age range, proportion of females, number of participants, and dosing regimens reported in the respective clinical trials. A total of 10 trials was conducted in the simulation to determine plasma drug concentrations over time. The model was considered

successfully verified if the predicted C_{max} and AUC values fell within the range and variations of the clinical observation data. The recently reported drug-drug interactions clinical trial between nirmatrelvir/ritonavir and midazolam (Cox *et al.*, 2023) was used to verify the nirmatrelvir/ritonavir model. Similarly, published clinical PK studies were used to verify the dexamethasone (Varis, 2000), clarithromycin (Chu *et al.*, 1993), and itraconazole (Uno *et al.*, 2006) models. The respective input parameters associated with the compound files described in table 2 was used for the model verification study. Additionally, the midazolam compound file in Simcyp (Sim-Midazolam) was used for nirmatrelvir/ritonavir model verification, and the associated input parameters for midazolam compound file is described in Supplementary Table S2. The demographic and dosing information associated with the respective clinical studies used for the model verification are described in table 3.

Results

Model verification

The predictive performance of the developed PBPK model for nirmatrelvir/ritonavir, dexamethasone, clarithromycin, and itraconazole compound files were in good agreement with the corresponding clinical observations (Figure 1 and Table 3). The PBPK model for nirmatrelvir/ritonavir accurately predicted the C_{max} and AUC with predicted/observed ratios of 1.02 and 0.99, respectively (Table 3), which falls within the reported % CV of 23% for C_{max} and 24% for AUC (Cox *et al.*, 2023). The ratios of predicted/observed values for dexamethasone C_{max} and AUC were 0.85 and 0.99, respectively (Table 3). These values align well with the clinical observations, which had a standard deviation of 16 ng/mL for C_{max} and 53 ng.hr/mL for AUC (Varis, 2000). The developed clarithromycin PBPK model had a predicted/observed ratio of 1.07 and 0.97 for C_{max} and AUC, respectively (Table 3), which is in good agreement with

17

clinical observations which had a standard deviation of 0.35 mg/L for C_{max} and 2.60 mg/L.hr for

AUC (Chu *et al.*, 1993). Similarly, the predicted/observed ratios for itraconazole's C_{max} and AUC

were 0.92 and 1.06, respectively, aligning with clinical observations that showed a standard

deviation of 87.3 ng/mL for C_{max} and 1159.6 ng.hr/mL for AUC (Uno *et al.*, 2006). The predicted

concentration-time profile plots closely matched the clinical observations (Figure 1),

demonstrating that the model accurately recovers plasma concentrations of nirmatrelvir/ritonavir,

dexamethasone, clarithromycin, and itraconazole.

Nirmatrelvir

In the healthy cohort, the concentration ratio of the fluid compartment in the low lobe of the right

lung ($C_{max,fluid}$) to plasma ($C_{max,plasma}$) was 0.34, while the ratio for the tissue mass compartment

($C_{max, tissue mass}$) in the same lung segment compared to $C_{max,plasma}$ was approximately 0.64, as

shown in Figure 2 and Table 4. Despite variations in the concurrent hepatic downregulation and

lung upregulation of CYP3A4 abundance among the outpatient, non-ICU, and ICU cohorts, the

concentration ratios remained similar to what was observed in the healthy cohort (Figure 2 and

Table 4). Across all three compartments, the highest percentage increase in the investigated PK

parameters was observed in the comparison between ICU and healthy cohorts, with an AUC_{plasma}

increase of approximately 56% in the ICU cohort relative to the healthy cohort (Table 5).

Furthermore, the percentage increase in AUC_{plasma} was always higher than $C_{max,plasma}$ across all

the six comparisons, although the increase was fairly negligible and revolved around 1-fold

(Table 5). Nevertheless, the percentage increase in $C_{max,fluid}$ and $C_{max, tissue mass}$ was consistent, and

it did not closely resemble the percentage increase in $C_{max,plasma}$ (Table 5). In the healthy cohort,

the $C_{max,plasma}$ of nirmatrelvir exceeded the $EC_{90,omicron}$ by 92-fold and the $EC_{90,delta}$ by

approximately 31-fold (Figure 2 and Table 6). In the ICU cohort, these concentrations reached

18

approximately 126-fold for the omicron variant and 42-fold for the delta variant (Figure 2 and Table 6). Within the right lung low lobe, the $C_{max,fluid}$ was approximately 32-fold and 11-fold higher than the $EC_{90,omicron}$ and $EC_{90,delta}$, respectively in the healthy cohort (Figure 2 and Table 6). In the ICU cohort, these concentrations eventually increased to about 41-fold for the omicron variant and approximately 14-fold for the delta variant, as illustrated in Figure 2 and detailed in Table 6. In the healthy cohort, the $C_{max,tissue\ mass}$ within the low lobe of the right lung was 59-fold higher than the $EC_{90,omicron}$ and approximately 20-fold higher than the $EC_{90,delta}$ (Figure 2 and Table 6). In the ICU cohort, these concentrations finally increased to approximately 76-fold for the omicron variant and 25-fold for the delta variant (Figure 2 and Table 6). In general, the fold change was more for the omicron variant than the delta variant across all three compartments (Table 6). When considering individual compartments, the fold changes were higher in the plasma, followed by tissue mass, and then fluid compartments (Figure 2 and Table 6). A noticeable overall increase in fold changes was observed from the healthy cohort to the ICU cohort, as indicated in Table 6. Additionally, there was no prominent differences in ritonavir plasma concentrations across the different patient cohorts (Supplementary Figure S1).

Dexamethasone

In the healthy cohort, the ratio of the $C_{max,fluid}$ in the low lobe of the right lung to $C_{max,plasma}$ was 0.25, while the ratio for the $C_{max,tissue\ mass}$ compartment in the same lung segment compared to $C_{max,plasma}$ was approximately 0.47 (Figure 3 and Table 4). Similar concentration ratios were maintained among the outpatient, non-ICU, and ICU cohorts despite the differences in the levels of hepatic downregulation and lung upregulation of CYP3A4 expression (Figure 3 and Table 4). Similar to the findings with nirmatrelvir, the most substantial percentage increase in the studied PK parameters across all three compartments occurred when comparing the ICU and healthy

cohorts (Table 5). Specifically, the AUC_{plasma} showed a 114% increase in the ICU cohort compared to the healthy cohort, as detailed in Table 5. This increase in AUC_{plasma} was about two times higher than the corresponding increase observed for nirmatrelvir. In the plasma compartment, the percentage increase in AUC consistently exceeded that of C_{max} by about 2-fold in all six comparisons, except for the ICU: healthy comparison, where the increase was approximately 3-fold (Table 5). This fold increase is about twice what was observed in nirmatrelvir. However, the percentage increase in C_{max} remained uniform for both the fluid and tissue mass compartments of the low lobe of the right lung, closely mirroring the pattern observed in plasma (Table 5). This consistency in lung compartmental C_{max} aligns with the observations for nirmatrelvir, as outlined in Table 5. However, the systemic and pulmonary dexamethasone C_{max} resemblance does not align with what was observed for nirmatrelvir (Table 5). In the healthy cohort, the $C_{max,plasma}$ exceeded the reported IC_{50} and IC_{90} of dexamethasone by around 30-fold and 3-fold, respectively (Figure 3 and Table 6). In the ICU cohort, these fold changes eventually reached 42-fold and approximately 5-fold (Figure 3 and Table 6). Within the right lung low lobe, the $C_{max,fluid}$ surpassed the IC_{50} and IC_{90} by about 7-fold and approximately 1-fold, respectively in the healthy cohort (Figure 3 and Table 6). Finally, these concentrations reached 10-fold and 1-fold above the IC_{50} and IC_{90}, respectively in the ICU cohort (Figure 3 and Table 6). The $C_{max,tissue\ mass}$ was about 14-fold and 2-fold above the IC_{50} and IC_{90}, respectively, in the healthy cohort. However, the ICU cohort had a fairly higher fold change of about 20-fold and 2-fold above the IC_{50} and IC_{90}, respectively (Figure 3 and Table 6). The fold changes, mirroring the pattern observed with nirmatrelvir, demonstrated higher levels in plasma, followed by tissue mass, and then fluid compartments, as detailed in Table 6. Notably, there was also an overall increase in fold changes from the healthy to ICU cohorts (Figure 3 and Table 6).

Clarithromycin

In the healthy cohort, the ratio of the $C_{max,fluid}$ in the low lobe of the right lung to $C_{max,plasma}$ was 0.57, while the ratio for the $C_{max,tissue\ mass}$ compartment in the same lung segment compared to $C_{max,plasma}$ was approximately 3.90 (Figure 4 and Table 4). Similar concentration ratios were observed among the outpatient, non-ICU, and ICU cohorts, despite the varying levels of hepatic downregulation and lung upregulation of CYP3A4 expression (Figure 4 and Table 4). However, these ratios were higher than what was observed in nirmatrelvir and dexamethasone. It was approximately 2-fold higher than what was observed in the fluid: plasma concentration ratios for nirmatrelvir and dexamethasone. The tissue mass: plasma concentration ratio was approximately 6-fold and 8-fold higher than what was observed for nirmatrelvir and dexamethasone, respectively. In all three compartments, the highest percentage increase in the studied PK parameters occurred when comparing the ICU and healthy cohorts (Table 5). This comparison revealed about 44% increase in AUC_{plasma} in the ICU cohort relative to the healthy cohort, as indicated in Table 5. This AUC_{plasma} increase is about 1.28 and 2.61 times lower than the corresponding increase observed for nirmatrelvir and dexamethasone, respectively. In the plasma compartment, the percentage increase in AUC consistently exceeded that of C_{max} by roughly 2-fold in all six comparisons (Table 5). However, the percentage increase in C_{max} remained similar for both the fluid and tissue mass compartments of the low lobe of the right lung, resembling the pattern observed in plasma (Table 5). The consistency in clarithromycin's lung compartmental C_{max} matches the patterns seen with nirmatrelvir and dexamethasone, whereas the similarity in systemic and pulmonary C_{max} is observed only with dexamethasone. In the healthy cohort, the $C_{max,plasma}$ of clarithromycin exceeded the $MIC_{90,S.pneumoniae}$ by 241-fold and reached 304-fold in the ICU cohort (Figure 4 and Table 6). Within the right lung low lobe, the $C_{max,fluid}$ was 138-fold

21

higher than the $MIC_{90,S.pneumoniae}$ in the healthy cohort and eventually reached a high of approximately 175-fold in the ICU cohort (Figure 4 and Table 6). Within the same lung segment, the $C_{max,tissue\ mass}$ was approximately 941-fold higher than the $MIC_{90,S.pneumoniae}$ in the healthy cohort and finally reached a high of 1189-fold in the ICU cohort (Figure 4 and Table 6). Contrary to what was observed for the investigated SARS-CoV-2 variants and nirmatrelvir, as well as dexamethasone, the fold changes in compartmental concentrations of clarithromycin relative to $MIC_{90,S.pneumoniae}$ were higher in the tissue mass, followed by plasma, and then fluid compartments (Figure 4 and Table 6). There was also a general upward trend in fold changes from healthy to ICU cohorts (Figure 4 and Table 6).

Itraconazole

In the healthy cohort, the ratio of $C_{max,fluid}$ compartment in the low lobe of the right lung to $C_{max,plasma}$ was approximately 0.02, while the ratio for the $C_{max,tissue\ mass}$ compartment in the same lung segment compared to $C_{max,plasma}$ was about 5.60, as shown in Figure 5 and Table 4. Despite differences in hepatic downregulation and lung upregulation of CYP3A4 expression, similar concentration ratios were maintained across the outpatient, non-ICU, and ICU cohorts (Figure 5 and Table 4). Nevertheless, these ratios were different from what was observed for nirmatrelvir, dexamethasone, and clarithromycin. For the fluid and plasma concentration ratios, it was less than what was observed for nirmatrelvir, dexamethasone, and clarithromycin by about 23, 17, and 38 times (Table 4). On the contrary, the tissue mass and plasma concentration ratios were about 9, 12, and 1 times higher than what was observed for nirmatrelvir, dexamethasone, and clarithromycin (Table 4). The most substantial percentage increase in the investigated PK parameters across all three compartments was observed in the comparison between the ICU and healthy cohorts (Table 5). This comparison showed approximately 196% rise in AUC_{plasma} in the

22

ICU cohort compared to the healthy cohort, as shown in Table 5. This AUC_{plasma} increase is about 3.5 and 4.5 times higher than what was observed for nirmatrelvir and clarithromycin, respectively, but slightly higher than the corresponding increase observed for dexamethasone (Table 5). In the plasma compartment, the percentage increase in AUC consistently surpassed that of C_{max} by approximately 1-fold across all six comparisons (Table 5). However, the percentage increase in C_{max} remained constant for both the fluid and tissue mass compartments of the low lobe of the right lung, mirroring the pattern observed in plasma (Table 5). The consistency in itraconazole's lung compartmental C_{max} matches the patterns seen with nirmatrelvir, dexamethasone, and clarithromycin, whereas the similarity in systemic and pulmonary C_{max} is observed only with dexamethasone and clarithromycin. In the healthy cohort, the $C_{max,plasma}$ of itraconazole exceeded the EC_{50} and EC_{90} of the investigated SARS-CoV-2 strain, hCoV-19/Germany/FI1103201/2020 by approximately 2-fold and 1-fold, respectively (Figure 5 and Table 6). These fold increases reached 6-fold and approximately 3-fold respectively in the ICU cohort (Figure 5 and Table 6). Within the low lobe of the right lung, both EC_{50} and EC_{90} were higher than the $C_{max,fluid}$ in the healthy cohort by about 28-fold and 61-fold, respectively (Figure 5 and Table 6). These fold changes eventually decreased to 10-fold and 23-fold in the ICU cohort (Figure 5 and Table 6). In the same lung segment, the $C_{max,tissue\ mass}$ was roughly 13-fold and approximately 6-fold higher than the EC_{50} and EC_{90} in the healthy cohort, respectively, eventually reaching a high of 35-fold above the EC_{50} and a high of about 16-fold above the EC_{90} in the ICU cohort (Figure 5 and Table 6). This is substantially different from what was observed for nirmatrelvir and the respective EC_{90}'s for the omicron and delta variants. Nirmatrelvir C_{max} was always several folds above the EC_{90} for the omicron and delta variants (Figure 2 and Table 6) compared to what was observed for itraconazole (Figure 5 and Table 6), although the SARS-

23

CoV-2 variants investigated were different. In contrast to the findings with the studied SARS-CoV-2 variants and nirmatrelvir, the fold changes in compartmental concentrations of itraconazole relative to the EC values, were more elevated in the tissue mass, followed by plasma, and then fluid compartments (Table 6). Additionally, there was an overall increasing trend in fold changes from the healthy to ICU cohorts (Figure 5 and Table 6).

Discussion

This present study demonstrates how COVID-19-mediated bidirectional simultaneous dysregulation of liver and lung CYP3A4 affects the systemic and pulmonary concentrations of four respiratory infectious disease drugs, aiming to identify target-organ-specific and patient cohort-specific factors that will guide the design of personalized treatments for at risk patients.

In this present study, it is evident that COVID-19-mediated upregulation of pulmonary CYP3A4 does not necessarily lead to a corresponding decrease in drug concentrations within the pulmonary compartments as anticipated (Figures 2 – 5). Rather, it is the COVID-19-mediated downregulation of hepatic CYP3A4 that is the primary determinant of both systemic and pulmonary drug concentrations across the different virtual patient cohorts, specifically healthy, outpatients, non-ICU, and ICU patients whose hepatic and lung CYP3A4 abundance were defined by clinical COVID-19-CYP3A4 interactions data. Unexpectedly, the downward trend of hepatic CYP3A4 abundance from healthy to ICU patients was associated with an upward trend of both systemic and pulmonary drug concentrations, despite the upward trend of lung CYP3A4 abundance in these patient cohorts (Figures 2 – 5). However, permeability appears to be a key factor in determining the influence of CYP3A4 dysregulation on systemic and pulmonary distribution profile for the investigated drugs (Tables 2 and 4). The higher a drug's permeability, the more its pulmonary distribution pattern in virtual patient cohorts will be influenced by

hepatic CYP3A4 dysregulation, and vice versa (Tables 2 and 4). Furthermore, the excessive accumulation of clarithromycin and itraconazole in the lung tissue mass compartment suggests that plasma measurements may not accurately reflect drug concentrations in the lung tissue (Figures 4 and 5, and Table 4).

Although the liver and lung are both eliminating organs, eliminating capacity is most substantial in the liver compared to the lung, especially for CYP3A4 whose lung activity is approximately 20% of hepatic activity (Anttila *et al.*, 1997). Moreover, the impact of hepatic CYP3A4 levels on the systemic and lung concentrations of these drugs will also vary based on the fraction of each drug metabolized by CYP3A4 ($f_{m,CYP3A4}$). The $f_{m,CYP3A4}$ increases progressively from clarithromycin through nirmatrelvir, dexamethasone, and finally itraconazole (Table 2). This trend is also reflected in their respective percentage increases in PK parameters, particularly C_{max} and AUC (Table 5), as well as their concentration-time profiles (Figures 2 – 5). Consequently, itraconazole shows the highest drug exposure in both systemic and pulmonary compartments across the cohorts, while clarithromycin shows the least (Table 5), reflecting the governing role of CYP3A4 in their respective metabolic pathways.

Evidently, the ICU cohort was the most affected, having the highest percentage increase in drug concentrations across all three compartments compared to the other cohorts (Table 5). Nirmatrelvir exposure was higher than the $EC_{90,omicron}$ and $EC_{90,delta}$ across all the investigated compartments with the plasma compartment taking the lead (Table 6). The paxlovid components, nirmatrelvir and ritonavir, remained unaffected due to ritonavir's inhibition of hepatic CYP3A4, resulting in stable systemic and pulmonary drug concentrations (Figure 2). However, CYP-mediated interactions are not recognized in the Simcyp lung model. Of all the patient cohorts, ICU patients had the most nirmatrelvir exposure than is required to clear the respective virus

25

variants (Figure 2 and Table 6). This may warrant further dosing adjustments for ICU patients with renal and/or hepatic impairments, as well as those with polypharmacy (Marzolini *et al.*, 2022), since ritonavir-mediated inhibition of CYP3A4 shifts the primary disposition of nirmatrelvir toward renal elimination and other secondary hepatic metabolic processes (Sagawa *et al.*, 2023).

Similarly, ICU patients were overexposed to dexamethasone relative to the investigated IC_{90} (Figure 3 and Table 6) potentially putting them at risk of opportunistic infections including the development of invasive pulmonary Aspergillosis. This association has been observed in some hospitalized COVID-19 patients who have been treated with dexamethasone (Skoglund *et al.*, 2021). Unexpectedly, clarithromycin $C_{max,plasma}$, $C_{max,fluid}$, and $C_{max,tissue\ mass}$ were about 304-fold, 175-fold, and 1189-fold higher than the MIC_{90} of the respiratory pathogen, *S.pneumoniae* (Figure 4 and Table 6), respectively in the ICU cohort. This over-exposure is important because clarithromycin causes idiosyncratic liver injury potentially through its potent inhibition of CYP3A4 that leads to elevated blood levels (LiverTox, 2012) and can be further compounded by COVID-19-mediated downregulation of hepatic CYP3A4, which may be clinically relevant for the treatment of community-acquired pneumonia (LiverTox, 2012; Dion and Ashurst, 2024).

Itraconazole is more concentrated in the tissue mass compartment compared to the fluid and plasma compartments (Figure 5 and Table 4). Interestingly, both the EC_{50} and EC_{90} are well above the C_{max} of itraconazole in the fluid compartment, with the EC_{90} taking the lead (Figure 5 and Table 6). This finding is significant because the fluid compartment contains the ELF, and drug concentrations in the ELF are clinically important for the effectiveness of COVID-19 treatments, as it may harbour SARS-CoV-2 virus (Pilla Reddy *et al.*, 2021). In a recent study, itraconazole did not reduce viral load in the lungs, stools, or ileum despite sufficient drug levels

26

in the bloodstream and lungs of SARS-CoV-2-infected hamsters (Liesenborghs *et al.*, 2021). It also failed to prevent viral transmission, culminating in the early termination of the corresponding clinical trial (Liesenborghs *et al.*, 2021). However, their study (Liesenborghs *et al.*, 2021) measured total itraconazole drug concentrations in the lung without investigating their concentrations in lung compartments, particularly the ELF (Pilla Reddy *et al.*, 2021) and alveolar epithelial cells (Rendeiro *et al.*, 2021) that are most affected by SARS-CoV-2 infection. In the SARS-CoV-2 infected hamster portion of their study, the authors reported that the high-dose regimen (70 mg/kg/day), reached lung concentrations that surpassed the EC_{50} required to combat SARS-CoV-2 (2115 ng/ml) and approached the EC_{90} level (6345 ng/mL) (Liesenborghs *et al.*, 2021). This current study suggests that itraconazole would not reach 30 ng/mL let alone 2115 ng/mL in the fluid compartment (Figure 5 and Table 6). This underscores the significance of measuring drug concentrations in target site compartments, and mass spectrometry imaging stands out as an excellent analytical tool for conducting such preclinical investigations (Nwabufo and Aigbogun, 2022). Further studies are needed to directly measure the concentrations of itraconazole in the ELF to determine whether insufficient concentrations are the primary reason for its limited efficacy for the treatment of SARS-CoV-2 infection.

The PBPK model verification demonstrated an excellent predictive accuracy for the plasma recovery of the investigated drugs (Figure 1 and Table 3), instilling a strong degree of confidence in its ability to deliver comparable predictive performance for the COVID-19-drug interactions study which could not be further verified due to the absence of corresponding clinical PK data. However, the COVID-19-drug interactions PBPK model was developed using existing clinical COVID-19-CYP3A4 interactions data (Le Carpentier *et al.*, 2022; Nwabufo *et al.*, 2024). Furthermore, evaluating the effects of additional pharmacological factors, such as membrane

drug transporters and intestinal metabolism, as well as pathophysiological attributes like the impact of COVID-19 on lung function and plasma proteins, were beyond the scope of this study as those have been previously investigated (Gaohua *et al.*, 2015; Rowland Yeo *et al.*, 2020). Studies like this one, which estimate tissue-specific data—particularly for hard-to-assess peripheral tissues such as the lungs, and special populations like patients with COVID-19-drug interactions—are currently made possible by PBPK modeling, making it easier to address complexities that are challenging to evaluate in clinical trials (Gallo, 2021). The outcome of this study can prove highly advantageous in designing drug treatments that considers patient-specific COVID-19-drug interactions liabilities to optimize both systemic and target site drug concentrations. More recently, PBPK modeling has been used to predict the optimal therapeutic concentrations of promising COVID-19 drugs in the human brain (Saleh *et al.*, 2023) and lung tissues (Rowland Yeo *et al.*, 2020; Gallo, 2021; Abla *et al.*, 2024). It is anticipated that as more clinical data become available, researchers can further verify and refine these tissue-specific predictions generated with PBPK modeling.

In conclusion, this PBPK modeling study have shown that hepatic CYP3A4 metabolism is the primary determinant of both systemic and pulmonary concentrations of the investigated drugs despite the concurrent COVID-19-mediated bidirectional dysregulation of liver and lung CYP3A4 expression. This suggest that COVID-19-CYP3A4 interactions in the liver may be more useful for guiding the design of personalized dosing regimens that achieves optimal pulmonary therapeutic concentrations for at risk patient populations. It was also evident that drug concentrations showed the most substantial increase in ICU patients as compared to the other cohorts. This rise was linked to the increased downregulation of hepatic CYP3A4, underscoring the importance of optimizing dosing regimens in ICU patients to enhance both efficacy and

safety profiles. We observed an increasing over-exposure of dexamethasone, nirmatrelvir, and clarithromycin with potential safety concerns, especially for ICU patients. On the contrary, there was a significant under-exposure of itraconazole in the lung fluid compartment with potential efficacy concerns for the treatment of COVID-19. Altogether, the findings from this present study and recent studies from our group and other groups have expanded scientific knowledge on COVID-19-drug interactions and provide a framework that can initially inform the design of personalized treatment plans for at risk patients (Nwabufo and Bendayan, 2022; Nwabufo, 2023).

Acknowledgments

Data Availability Statement

The author declares that all the data supporting the findings of this study are contained within the

paper. All additional information can be directed to Chukwunonso.nwabufo@mail.utoronto.ca

Authorship Contributions

Participated in research design: Nwabufo

Conducted experiments: Nwabufo

Contributed new reagents or analytic tools: Nwabufo

Performed data analysis: Nwabufo

Wrote or contributed to the writing of the manuscript: Nwabufo

References

Abla N, Almond LM, Bonner JJ, Richardson N, Wells TNC, and Möhrle JJ (2024) PBPK-led assessment of antimalarial drugs as candidates for Covid-19: Simulating concentrations at the site of action to inform repurposing strategies. *Clinical Translational Sci* **17**:e13865.

Anttila S, Hukkanen J, Hakkola J, Stjernvall T, Beaune P, Edwards RJ, Boobis AR, Pelkonen O, and Raunio H (1997) Expression and localization of CYP3A4 and CYP3A5 in human lung. *Am J Respir Cell Mol Biol* **16**:242–249.

Bösmüller H, Matter M, Fend F, and Tzankov A (2021) The pulmonary pathology of COVID-19. *Virchows Arch* **478**:137–150.

Chu S -y., Granneman GR, Pichotta PJ, Decourt JPh, Girault J, and Fourtillan JB (1993) Effect of Moderate or Severe Hepatic Impairment on Clarithromycin Pharmacokinetics. *The Journal of Clinical Pharma* **33**:480–485.

Cox DS, Rehman M, Khan T, Ginman K, Salageanu J, LaBadie RR, Wan K, and Damle B (2023) Effects of nirmatrelvir/ritonavir on midazolam and dabigatran pharmacokinetics in healthy participants. *Brit J Clinical Pharma* **89**:3352–3363.

Dahl AR, and Hadley WM (1991) Nasal Cavity Enzymes Involved in Xenobiotic Metabolism: Effects on the Toxicity of Inhalants. *Critical Reviews in Toxicology* **21**:345–372.

Dion CF, and Ashurst JV (2024) Streptococcus pneumoniae, in *StatPearls* p, StatPearls Publishing, Treasure Island (FL).

European Medicines Agency (2021) Assessment report on paxlovid use in COVID-19.

Frisoni P, Neri M, D'Errico S, Alfieri L, Bonuccelli D, Cingolani M, Di Paolo M, Gaudio RM, Lestani M, Marti M, Martelloni M, Moreschi C, Santurro A, Scopetti M, Turriziani O, Zanon M, Scendoni R, Frati P, and Fineschi V (2022) Cytokine storm and histopathological findings in 60 cases of COVID-19-related death: from viral load research to immunohistochemical quantification of major players IL-1β, IL-6, IL-15 and TNF-α. *Forensic Sci Med Pathol* **18**:4–19.

Gallo JM (2021) Hybrid physiologically-based pharmacokinetic model for remdesivir: Application to SARS-CoV-2. *Clinical and Translational Science* **14**.

Gaohua L, Wedagedera J, Small B, Almond L, Romero K, Hermann D, Hanna D, Jamei M, and Gardner I (2015) Development of a Multicompartment Permeability-Limited Lung PBPK Model and Its Application in Predicting Pulmonary Pharmacokinetics of Antituberculosis Drugs. *CPT Pharmacom & Syst Pharma* **4**:605–613.

Gregoire M, Le Turnier P, Gaborit BJ, Veyrac G, Lecomte R, Boutoille D, Canet E, Imbert B-M, Bellouard R, and Raffi F (2020) Lopinavir pharmacokinetics in COVID-19 patients. *J Antimicrob Chemother* **75**:2702–2704.

33

Hardy DJ, Guay DRP, and Jones RN (1992) Clarithromycin, a unique macrolide. *Diagnostic Microbiology and Infectious Disease* **15**:39–53.

Hoffmann M, Kleine-Weber H, Schroeder S, Krüger N, Herrler T, Erichsen S, Schiergens TS, Herrler G, Wu N-H, Nitsche A, Müller MA, Drosten C, and Pöhlmann S (2020) SARS-CoV-2 Cell Entry Depends on ACE2 and TMPRSS2 and Is Blocked by a Clinically Proven Protease Inhibitor. *Cell* **181**:271-280.e8.

Hou YJ, Okuda K, Edwards CE, Martinez DR, Asakura T, Dinnon KH, Kato T, Lee RE, Yount BL, Mascenik TM, Chen G, Olivier KN, Ghio A, Tse LV, Leist SR, Gralinski LE, Schäfer A, Dang H, Gilmore R, Nakano S, Sun L, Fulcher ML, Livraghi-Butrico A, Nicely NI, Cameron M, Cameron C, Kelvin DJ, de Silva A, Margolis DM, Markmann A, Bartelt L, Zumwalt R, Martinez FJ, Salvatore SP, Borczuk A, Tata PR, Sontake V, Kimple A, Jaspers I, O'Neal WK, Randell SH, Boucher RC, and Baric RS (2020) SARS-CoV-2 Reverse Genetics Reveals a Variable Infection Gradient in the Respiratory Tract. *Cell* **182**:429-446.e14.

Kumar S, Sarma P, Kaur Hardeep, Prajapat M, Bhattacharyya A, Avti P, Sehkhar N, Kaur Harpinder, Bansal S, Mahendiratta S, Mahalmani VM, Singh H, Prakash A, Kuhad A, and Medhi B (2021) Clinically relevant cell culture models and their significance in isolation, pathogenesis, vaccine development, repurposing and screening of new drugs for SARS-CoV-2: a systematic review. *Tissue and Cell* **70**:101497.

Le Carpentier EC, Canet E, Masson D, Martin M, Deslandes G, Gaultier A, Dailly É, Bellouard R, and Gregoire M (2022) Impact of Inflammation on Midazolam Metabolism in Severe COVID-19 Patients. *Clin Pharmacol Ther* **112**:1033–1039.

Lenoir C, Terrier J, Gloor Y, Curtin F, Rollason V, Desmeules JA, Daali Y, Reny J, and Samer CF (2021) Impact of SARS-CoV-2 Infection (COVID-19) on Cytochromes P450 Activity Assessed by the Geneva Cocktail. *Clin Pharma and Therapeutics* **110**:1358–1367.

Liesenborghs L, Spriet I, Jochmans D, Belmans A, Gyselinck I, Teuwen L-A, Ter Horst S, Dreesen E, Geukens T, Engelen MM, Landeloos E, Geldhof V, Ceunen H, Debaveye B, Vandenberk B, Van Der Linden L, Jacobs S, Langendries L, Boudewijns R, Do TND, Chiu W, Wang X, Zhang X, Weynand B, Vanassche T, Devos T, Meyfroidt G, Janssens W, Vos R, Vermeersch P, Wauters J, Verbeke G, De Munter P, Kaptein SJF, Rocha-Pereira J, Delang L, Van Wijngaerden E, Neyts J, and Verhamme P (2021) Itraconazole for COVID-19: preclinical studies and a proof-of-concept randomized clinical trial. *eBioMedicine* **66**:103288.

LiverTox (2012) *LiverTox: Clinical and Research Information on Drug-Induced Liver Injury*, National Institute of Diabetes and Digestive and Kidney Diseases, Bethesda (MD).

Marzolini C, Kuritzkes DR, Marra F, Boyle A, Gibbons S, Flexner C, Pozniak A, Boffito M, Waters L, Burger D, Back DJ, and Khoo S (2022) Recommendations for the Management of Drug–Drug Interactions Between the COVID -19 Antiviral Nirmatrelvir/Ritonavir (Paxlovid) and Comedications. *Clin Pharma and Therapeutics* **112**:1191–1200.

Montanha MC, Cottura N, Booth M, Hodge D, Bunglawala F, Kinvig H, Grañana-Castillo S, Lloyd A, Khoo S, and Siccardi M (2022) PBPK Modelling of Dexamethasone in Patients With COVID-19 and Liver Disease. *Front Pharmacol* **13**:814134.

Nwabufo C, Luc J, McGeer A, Hirota J, Mubareka S, Doxey A, and Moraes T (2024) COVID-19 Severity Gradient Differentially Dysregulates Clinically Relevant Drug Processing Genes in Nasopharyngeal Swab Samples. *Brit J Clinical Pharma* bcp.16124.

Nwabufo CK (2023) Mirvetuximab soravtansine in ovarian cancer therapy: expert opinion on pharmacological considerations. *Cancer Chemother Pharmacol*, doi: 10.1007/s00280-023-04575-y.

Nwabufo CK, and Aigbogun OP (2022) Potential application of mass spectrometry imaging in pharmacokinetic studies. *Xenobiotica* **52**:811–827.

Nwabufo CK, and Bendayan R (2022) Pharmacokinetic considerations to optimize clinical outcomes for COVID-19 drugs. *Trends Pharmacol Sci* **43**:1041–1054.

Nwabufo CK, Hoque MdT, Yip L, Khara M, Mubareka S, Pollanen MS, and Bendayan R (2023) SARS-CoV-2 infection dysregulates the expression of clinically relevant drug metabolizing enzymes in Vero E6 cells and membrane transporters in human lung tissues. *Front Pharmacol* **14**:1124693.

Pilla Reddy V, El-Khateeb E, Jo H, Giovino N, Lythgoe E, Sharma S, Tang W, Jamei M, and Rastomi-Hodjegan A (2021) Pharmacokinetics under the COVID-19 storm. *Br J Clin Pharmacol* 1–29.

Reed CJ (1993) Drug Metabolism in the Nasal Cavity: Relevance to Toxicology. *Drug Metabolism Reviews* **25**:173–205.

Rendeiro AF, Ravichandran H, Bram Y, Chandar V, Kim J, Meydan C, Park J, Foox J, Hether T, Warren S, Kim Y, Reeves J, Salvatore S, Mason CE, Swanson EC, Borczuk AC, Elemento O, and Schwartz RE (2021) The spatial landscape of lung pathology during COVID-19 progression. *Nature* **593**:564–569.

Rosales R, McGovern BL, Rodriguez ML, Rai DK, Cardin RD, Anderson AS, PSP study group, Sordillo EM, Van Bakel H, Simon V, García-Sastre A, and White KM (2022) *Nirmatrelvir, Molnupiravir, and Remdesivir maintain potent* in vitro *activity against the SARS-CoV-2 Omicron variant*, Microbiology.

Rowland Yeo K, Zhang M, Pan X, Ban Ke A, Jones HM, Wesche D, and Almond LM (2020) Impact of Disease on Plasma and Lung Exposure of Chloroquine, Hydroxychloroquine and Azithromycin: Application of PBPK Modeling. *Clin Pharma and Therapeutics* **108**:976–984.

Russell LE, Zhou Y, Almousa AA, Sodhi JK, Nwabufo CK, and Lauschke VM (2021) Pharmacogenomics in the era of next generation sequencing – from byte to bedside. *Drug Metabolism Reviews* **53**:253–278.

Sagawa K, Lin J, Jaini R, and Di L (2023) Physiologically-Based Pharmacokinetic Modeling of PAXLOVID^{TM} with First-Order Absorption Kinetics. *Pharm Res* **40**:1927–1938.

Saleh MAA, Hirasawa M, Sun M, Gülave B, Elassaiss-Schaap J, and De Lange ECM (2023) The PBPK LeiCNS-PK3.0 framework predicts Nirmatrelvir (but not Remdesivir or Molnupiravir) to achieve effective concentrations against SARS-CoV-2 in human brain cells. *European Journal of Pharmaceutical Sciences* **181**:106345.

Salerno DM, Kovac D, Corbo H, Jennings DL, Lee J, Choe J, Scheffert J, Hedvat J, Chen J, Tsapepas D, Rosenblatt R, Samstein B, Halazun K, Verna E, Pereira M, Brennan C, Husain SA, Mohan S, and Brown RS (2021) SARS-CoV-2 infection increases tacrolimus concentrations in solid-organ transplant recipients. *Clin Transplant* **35**:e14193.

Schloer S, Brunotte L, Mecate-Zambrano A, Zheng S, Tang J, Ludwig S, and Rescher U (2021) Drug synergy of combinatory treatment with remdesivir and the repurposed drugs fluoxetine and itraconazole effectively impairs SARS-CoV-2 infection in vitro. *British J Pharmacology* **178**:2339–2350.

Skoglund E, Kum A, Mac A, and Nguyen M (2021) 334. Impact of Overall Dexamethasone Exposure on Development of Invasive Pulmonary Aspergillosis in Hospitalized Patients with COVID-19. *Open Forum Infectious Diseases* **8**:S272–S272.

Uno T, Shimizu M, Sugawara K, and Tateishi T (2006) Sensitive Determination of Itraconazole and Its Active Metabolite in Human Plasma by Column-switching High-performance Liquid Chromatography With Ultraviolet Detection: *Therapeutic Drug Monitoring* **28**:526–531.

Van Damme E, De Meyer S, Bojkova D, Ciesek S, Cinatl J, De Jonghe S, Jochmans D, Leyssen P, Buyck C, Neyts J, and Van Loock M (2021) In vitro activity of itraconazole against SARS-CoV-2. *Journal of Medical Virology* **93**:4454–4460.

Varis T (2000) The cytochrome P450 3A4 inhibitor itraconazole markedly increases the plasma concentrations of dexamethasone and enhances its adrenal-suppressant effect. *Clinical Pharmacology & Therapeutics* **68**:487–494.

Ziegler CGK, Allon SJ, Nyquist SK, Mbano IM, Miao VN, Tzouanas CN, Cao Y, Yousif AS, Bals J, Hauser BM, Feldman J, Muus C, Wadsworth MH, Kazer SW, Hughes TK, Doran B, Gatter GJ, Vukovic M, Taliaferro F, Mead BE, Guo Z, Wang JP, Gras D, Plaisant M, Ansari M, Angelidis I, Adler H, Sucre JMS, Taylor CJ, Lin B, Waghray A, Mitsialis V, Dwyer DF, Buchheit KM, Boyce JA, Barrett NA, Laidlaw TM, Carroll SL, Colonna L, Tkachev V, Peterson CW, Yu A, Zheng HB, Gideon HP, Winchell CG, Lin PL, Bingle CD, Snapper SB, Kropski JA, Theis FJ, Schiller HB, Zaragosi L-E, Barbry P, Leslie A, Kiem H-P, Flynn JL, Fortune SM, Berger B, Finberg RW, Kean LS, Garber M, Schmidt AG, Lingwood D, Shalek AK, Ordovas-Montanes J, HCA Lung Biological Network. Electronic address: lung-network@humancellatlas.org, and HCA Lung Biological Network (2020) SARS-CoV-2 Receptor ACE2 Is an Interferon-Stimulated Gene in Human Airway Epithelial Cells and Is Detected in Specific Cell Subsets across Tissues. *Cell* **181**:1016-1035.e19.

Footnotes

Conflict of interest

Chukwunonso K. Nwabufo was a former employee of Gilead Sciences and was involved in the development of remdesivir and lenacapavir. Chukwunonso K. Nwabufo is employed by OneDrug Inc. The author does not have any conflicting interests associated with this research.

Scientific meeting presentations

Both oral and poster presentations of this research work was delivered by Chukwunonso K. Nwabufo at the 2024 Annual Meeting of the American College of Clinical Pharmacology (ACCP). Therefore, the accepted abstract will be published online in ACCP's Clinical Pharmacology in Drug Development Journal. The abstract was also selected for the ACCP/International Society of Pharmacometrics Special Interest Group Student Abstract Award. Furthermore, Chukwunonso K. Nwabufo delivered an oral presentation of this research work at the 2024 Translational Medicine Symposium of the Hospital for Sick Children Research Institute. Additionally, an abstract originating from this work was also selected for oral presentation at the upcoming 2024 American Association of Pharmaceutical Scientists Pharmsci 360 meeting.

Figure Legends

Figure 1. Predicted versus observed pharmacokinetic profile of nirmatrelvir/ritonavir, dexamethasone, clarithromycin, and itraconazole in the plasma compartment. Simcyp version 22.1 was used to simulate the plasma concentrations of nirmatrelvir/ritonavir, dexamethasone, clarithromycin, and itraconazole. The nirmatrelvir/ritonavir virtual trial involved 10 participants aged 21 to 50 years, with 8.3% being females while dexamethasone trial involved 8 participants aged between 20 to 42 years with 87.5% being females. The clarithromycin trial involved 6 participants aged between 45 to 64 years with 50% being females while itraconazole trial included 8 participants aged between 22 to 34 years with no female participants. The nirmatrelvir/ritonavir cohort received oral nirmatrelvir tablets at a dosage of 300 mg twice daily and ritonavir at 100 mg twice daily, both administered for a duration of 5 days with a single dose of 2 mg midazolam on the 5th day. The dexamethasone cohort received a single oral administration of 4.5 mg dexamethasone. The clarithromycin cohort received an oral administration of 250 mg clarithromycin every 12 hours for a total of 5 doses while 200 mg itraconazole once daily for 6 days was orally administered to the itraconazole cohort. The simulated pharmacokinetic profiles are represented by black solid lines while the observed clinical data are represented by orange discrete points. The two gray boundary lines represent the 5th and 95th percentile. For nirmatrelvir/ritonavir, the data are presented as geometric means, whereas for dexamethasone, clarithromycin, and itraconazole, the data are presented as mean values.

Figure 2. Pharmacokinetic profile of nirmatrelvir/ritonavir in the plasma compartment (A), fluid (B), and tissue mass (C) compartments of the right lung low lobe. Simcyp version 22.1 was used to simulate the systemic and pulmonary concentrations of nirmatrelvir/ritonavir in

a virtual trial involving 12 participants aged 21 to 50 years, with 8.3% being females. The participants were stratified into four cohorts comprising healthy individuals (light gray) and COVID-19 patients with varying disease severity including outpatients (green), non-ICU (orange), and ICU (red) cohorts. In these participant cohorts, their CYP3A4 abundance levels were downregulated in the liver and upregulated in the lung according to the clinical COVID-19 – CYP3A4 expression and activity data (Table 1). Permeability-limited lung model was activated with the primary goal of accounting for lung CYP3A4 metabolism without altering permeability parameters. The participants received nirmatrelvir tablets at a dosage of 300 mg twice daily and ritonavir at 100 mg twice daily, both administered for a duration of 5 days. The EC_{90} of nirmatrelvir for the omicron (25 ng/mL) and delta (74.5 ng/mL) variants of the SARS-CoV-2 virus are shown in dark blue and light blue dashed lines, respectively. The black solid line represents nirmatrelvir concentrations in the presence of ritonavir-mediated interactions with CYP3A4.

Figure 3. Pharmacokinetic profile of dexamethasone in the plasma compartment (A), fluid (B), and tissue mass (C) compartments of the right lung low lobe. Simcyp version 22.1 was used to simulate the systemic and pulmonary concentrations of dexamethasone in a virtual trial involving 100 participants aged between 18 to 60 years with 50% being females. The participants were stratified into four cohorts comprising healthy individuals (light gray) and COVID-19 patients with varying disease severity including outpatients (green), non-ICU (orange), and ICU (red) cohorts. In these participant cohorts, their CYP3A4 abundance levels were downregulated in the liver and upregulated in the lung according to the clinical COVID-19 – CYP3A4 expression and activity data (Table 1). Permeability-limited lung model was activated with the primary goal of accounting for lung CYP3A4 metabolism without altering permeability

39

parameters. The participants received an oral administration of 6 mg dexamethasone once a day for 10 days. The $1C_{50}$ (1.25 ng/mL) and IC_{90} (11.20 ng/mL) of dexamethasone for COVID-19 are shown in dark gold and black dashed lines, respectively.

Figure 4. Pharmacokinetic profile of clarithromycin in the plasma compartment (A), fluid (B), and tissue mass (C) compartments of the right lung low lobe. Simcyp version 22.1 was used to simulate the systemic and pulmonary concentrations of clarithromycin in a virtual trial involving 200 participants aged between 20 to 50 years with 50% being females. The participants were stratified into four cohorts comprising healthy individuals (light gray) and COVID-19 patients with varying disease severity including outpatients (green), non-ICU (orange), and ICU (red) cohorts. In these participant cohorts, their CYP3A4 abundance levels were downregulated in the liver and upregulated in the lung according to the clinical COVID-19 – CYP3A4 expression and activity data (Table 1). Permeability-limited lung model was activated with the primary goal of accounting for lung CYP3A4 metabolism without altering permeability parameters. The participants received an oral administration of 500 mg clarithromycin every 12 hours for a total of 8 doses. The $M1C_{90}$ (15 ng/mL) of clarithromycin for the respiratory pathogen, *Streptococcus pneumoniae* are shown in dark red dashed lines.

Figure 5. Pharmacokinetic profile of itraconazole in the plasma compartment (A), fluid (B), and tissue mass (C) compartments of the right lung low lobe. Simcyp version 22.1 was used to simulate the systemic and pulmonary concentrations of itraconazole in a virtual trial involving 260 participants aged between 23 to 50 years with 50% being females. The participants were stratified into four cohorts comprising healthy individuals (light gray) and COVID-19 patients with varying disease severity including outpatients (green), non-ICU (orange), and ICU (red) cohorts. In these participant cohorts, their CYP3A4 abundance levels were downregulated in the

40

liver and upregulated in the lung according to the clinical COVID-19 – CYP3A4 expression and activity data (Table 1). Permeability-limited lung model was activated with the primary goal of accounting for lung CYP3A4 metabolism without altering permeability parameters. The participants received an oral administration of 200 mg of itraconazole twice daily for a total of 10 doses. The EC_{50} (275.20 ng/mL) and EC_{90} (613.87 ng/mL) of itraconazole for a strain of SARS-CoV-2 known as hCoV-19/Germany/FI1103201/2020, which contains the D614G mutation in the spike protein are shown in purple and dark green dashed lines, respectively. These dashed lines are not included in the fluid compartment because they are much higher than itraconazole concentrations within that compartment.

Tables

Table 1. Estimated CYP3A4 expression levels within lung and liver tissues

Compartments	Variables	CYP3A4 Expression Levels in Patient Cohorts			
		Healthy	Outpatient	Non-ICU	ICU
Lung	% CYP3A4 nasopharyngeal expression	100.00	109.51	112.75	111.76
	Estimated CYP3A4 abundance levels (pmol/mg)	27.40	30.01	30.89	30.62
Liver	Plasma CRP concentration (mg/L)	<50	50 -150	150 - 250	>250
	% CYP3A4 activity levels	100.00	66.00	53.00	33.00
	Estimated CYP3A4 abundance levels (pmol/mg)	137.00	90.42	72.61	45.21

Table 2. Input parameters for the PBPK model of four respiratory infectious disease drugs

Categories and Parameters	Nirmatrelvir	Ritonavir	Dexamethasone	Clarithromycin	Itraconazole
Physicochemical properties					
MW (g/mol)	499.5	721	329.47	748	705.6
LogP	1.84	3.9	1.84	1.7	4.47
pKa 1	—	1.8	—	8.99	4.28
pKa 2	—	2.6	—	—	—
B/P	0.6	0.587	0.93	1	0.58
Compound type	Neutral	Diprotic base	Neutral	Monoprotic base	Monoprotic base
f_{up}	0.31	0.015	0.24	0.18	0.016
Absorption					
k_a (h^{-1})	0.55	0.45	0.8	2.42	0.2
f_a	0.73	0.5	1	1	1
Lag time (h)	—	—	0.4	0.26	—
$f_{u,gut}$, Q_{gut} (L/h)	1, 10	0.015, 19.127	0.24, 13.463	1, 10.375	0.016, 18.32
Absorption model	First-order	First-order	First-order	First-order	First-order
Distribution					
V_{ss} (L/kg) method 2	0.48203	0.40851	1.0343	5.7136	10.502

Kp scalar	0.48	0.066	1.4	1.3	0.4393
Distribution model	Full PBPK	Full PBPK	Full PBPK	Full PBPK	Full PBPK
Elimination					
$f_{m,CYP3A4}$	0.85	—	0.86	0.74	1.00
$f_{u,mic}$	1	1	1	1	1
$CL_{int,CYP3A4}$ (µl/min/pmol CYP enzymes)	0.148	—	0.15	—	—
$CL_{int,CYP3A4Lung}$ (µl/min/pmol CYP enzymes)	0.148	—	0.15	—	—
CL_R (L/h)	3.4	0.53	0.39	8.05	—
Other HLM CL_{int} (µl/min/mg)	3.23	75	2.28	—	—
$V_{max,CYP3A4}$ (pmol/min/pmol microsomal protein)	—	1.37	—	10.04	0.065
$V_{max,CYP2D6}$ (pmol/min/pmol microsomal protein)	—	0.7	—	—	—
$V_{max,CYP3A5}$ (pmol/min/pmol microsomal protein)	—	1	—	—	—
$V_{max, CYP3A4Lung}$ (pmol/min/pmol microsomal protein)	—	—	—	10.04	0.065
$K_m(K_s)$ CYP3A4 (µM)	—	0.07	—	22.3	0.0039
$K_m(K_s)$ CYP2D6 (µM)	—	1	—	—	—
$K_m(K_s)$ CYP3A5 (µM)	—	0.05	—	—	—

$K_m(K_s)$ CYP3A4Lung (μM)	—	—	—	22.3	0.0039
CYP-mediated interactions					
$K_{i,CYP3A4}$ (μM)	22.6	0.00194	—	10	0.0013
$K_{app,CYP3A4}$ (μM)	13.9	0.18	—	12	—
$k_{inact, CYP3A4}$ (h^{-1})	0.99	19.80	—	2.13	—
$Ind_{max, CYP3A4}$ (fold)	9.74	68.50	6.7	1	—
$IndC_{50, CYP3A4}$ (μM)	19.04	1	0.1	—	—
γ CYP3A4	1.63	1	—	—	—
$K_{i,CYP3A5}$ (μM)	—	0.00194	—	—	—
$K_{app, CYP3A5}$ (μM)	—	0.18	—	—	—
$k_{inact, CYP3A5}$ (h^{-1})	—	19.80	—	—	—
$Ind_{max, CYP3A5}$ (fold)	—	68.50	—	—	—
$IndC_{50, CYP3A5}$ (μM)	—	1	—	—	—
γ CYP3A5	—	1	—	—	—
$K_{i,CYP2D6}$ (μM)	—	0.04	—	—	—
$Ind_{max, CYP2C9}$ (fold)	—	3.33	—	—	—
$IndC_{50, CYP2C9}$ (μM)	—	0.07	—	—	—
Transporter-mediated interactions					
Gut Apical P-gp K_i (μM)	55.2	0.03	—	4	0.00939

Gut Apical OCT1 K_i (μM)	138.1	—	—	—	—
Gut Apical BCRP K_i (μM)	—	—	—	411	1.04
Liver Sinusoidal OATP1B1 K_i (μM)	44.4	—	—	0.35	—
Liver Sinusoidal OATP1B3 K_i (μM)	283.2	—	—	0.7	0.71
Liver Sinusoidal OATP2B1 K_i (μM)	—	—	—	—	2.43
Liver Sinusoidal OCT1 K_i (μM)	138.1	—	—	—	—
Liver Canalicular P-gp K_i (μM)	55.2	0.03	—	4	0.00939
Liver Canalicular MATE1 K_i (μM)	111.7	—	—	—	—
Liver Canalicular BCRP K_i (μM)	—	—	—	411	1.04
Kidney Apical P-gp K_i (μM)	55.2	—	—	—	—
Kidney Apical MATE1 K_i (μM)	111.7	—	—	—	—
Kidney Basal OCT2 K_i (μM)	954.5	—	—	—	—
Kidney Basal OAT3 K_i (μM)	520.6	—	—	—	—

Permeability-limited lung model

Henry's Constant (Pa m^3/mol)	1.0×10^{-37}	—	1.0×10^{-37}	1.0×10^{-37}	1.0×10^{-37}
Lung effective permeability (10^{-4} cm/s)	0.07631	—	1	1	1
fu_{mass}	0.5361	—	0.5361	0.11714	0.0027551
fu_{fluid}	1	—	1	1	1

Demographic and clinical profile of virtual clinical trial

Number of participants	12		100	200	260
Age range (years)	21-50		18-60	20-50	23-50
% female	8.3		50	50	50
Dose (mg)	300	100	6	500	200
Dosing frequency (day^{-1})	Twice	Twice	Once	Twice	Twice
Number of doses	9	9	10	8	10
Route of administration	Oral				
Effective drug concentrations for respiratory pathogens of interest					
$EC_{90,omicron}$ (ng/mL)	25	—	—	—	—
$EC_{90,delta}$ (ng/mL)	74.5	—	—	—	—
$IC_{50,COVID-19}$ (ng/mL)	—	—	1.25	—	—
$IC_{90,COVID-19}$ (ng/mL)	—	—	11.20	—	—
$MIC_{90,S.pneumoniae}$ (ng/mL)	—	—	—	15	—
$EC_{50,hCoV-19/Germany/FI1103201/2020}$ (ng/mL)	—	—	—	—	275.20
$EC_{90,hCoV-19/Germany/FI1103201/2020}$ (ng/mL)	—	—	—	—	613.87

Table 3. Clinical study design information used for PBPK model verification and corresponding results

Number of participants	Age range (years), % Female	Dosing Regimens	Observed		Predicted		Predicted/Observed	
			C_{max} (ng/mL)	AUC (ng.hr/mL)	C_{max} (ng/mL)	AUC (ng.hr/mL)	C_{max}	AUC
10	21-50, 8.3	300 mg nirmatrelvir tablet BID 5 days; 100 mg ritonavir BID 5 days; 2 mg midazolam single dose on day 5	3875.00	30680.00	3963.79	30262.15	1.02	0.99
8	20-42, 87.5	4.5 mg dexamethasone single dose	38.00	239.00	32.40	237.36	0.85	0.99
6	45-64, 50	250 mg clarithromycin Q12h for 5 doses	1520.00	9290.00	1630.00	9030.00	1.07	0.97
8	22-34, 0	200 mg itraconazole QD for 6 days	287.70	3485.50	264.03	3679.70	0.92	1.06

Table 4. Systemic and pulmonary concentration ratios of the investigated drugs across different cohorts

Drugs	Cohorts	Cmax (ng/mL)			Cmax Ratios	
		Plasma	Right lung lower lobe fluid	Right lung lower lobe tissue mass	Fluid: plasma ratio	Tissue mass: plasma ratio
Nirmatrelvir	Healthy	2308.36	791.45	1476.31	0.34	0.64
	Outpatient	2702.35	897.35	1673.84	0.33	0.62
	Non-ICU	2868.55	941.66	1756.49	0.33	0.61
	ICU	3137.48	1016.51	1896.11	0.32	0.60
Dexamethasone	Healthy	37.24	9.34	17.42	0.25	0.47
	Outpatient	42.99	10.73	20.01	0.25	0.47
	Non-ICU	46.01	11.46	21.38	0.25	0.46
	ICU	52.60	13.07	24.38	0.25	0.46
Clarithromycin	Healthy	3619.91	2073.52	14115.62	0.57	3.90
	Outpatient	4067.99	2308.88	15722.83	0.57	3.87
	Non-ICU	4250.93	2403.54	16371.43	0.57	3.85
	ICU	4562.22	2618.97	17837.99	0.57	3.91
Itraconazole	Healthy	651.43	10.00	3627.33	0.02	5.57
	Outpatient	1027.71	15.89	5762.10	0.02	5.61
	Non-ICU	1248.82	19.36	7020.25	0.02	5.62
	ICU	1712.59	26.69	9677.07	0.02	5.65

Table 5. Percentage increases in pharmacokinetic parameters of the investigated drugs across different compartments

| Drugs	Compartments	Pharmacokinetic Parameters	Percentage increases (%)					
			Outpatient: Healthy	Non-ICU: Healthy	ICU: Healthy	Non-ICU: Outpatient	ICU: Outpatient	ICU: Non-ICU
Nirmatrelvir	Plasma	C_{max} (ng/mL)	17.07	24.27	35.92	6.15	16.10	9.38
		AUC (ng.hr/mL)	25.44	36.73	55.83	9.00	24.23	13.97
	Right lung low lobe fluid	C_{max} (ng/mL)	13.38	18.98	28.44	4.94	13.28	7.95
	Right lung low lobe tissue mass	C_{max} (ng/mL)	13.38	18.98	28.44	4.94	13.28	7.95
Dexamethasone	Plasma	C_{max} (ng/mL)	15.45	23.53	41.23	7.00	22.34	14.33
		AUC (ng.hr/mL)	35.34	57.50	114.29	16.37	58.33	36.06
	Right lung low lobe fluid	C_{max} (ng/mL)	14.86	22.69	39.95	6.81	21.84	14.07
	Right lung low lobe tissue mass	C_{max} (ng/mL)	14.86	22.69	39.95	6.81	21.84	14.07
Clarithromycin	Plasma	C_{max} (ng/mL)	12.38	17.43	26.03	4.50	12.15	7.32
		AUC (ng.hr/mL)	20.19	28.92	43.75	7.27	19.60	11.50
	Right lung low lobe fluid	C_{max} (ng/mL)	11.35	15.92	26.31	4.10	13.43	8.96
	Right lung low lobe tissue mass	C_{max} (ng/mL)	11.39	15.98	26.37	4.12	13.45	8.96
Itraconazole	Plasma	C_{max} (ng/mL)	57.76	91.70	162.90	21.51	66.64	37.14
		AUC (ng.hr/mL)	68.12	108.93	195.67	24.28	75.87	41.52
	Right lung low lobe fluid	C_{max} (ng/mL)	58.85	93.54	166.78	21.83	67.94	37.85
	Right lung low lobe tissue mass	C_{max} (ng/mL)	58.85	93.54	166.78	21.83	67.94	37.85

Table 6. Fold changes between intercompartmental drug concentrations and effective concentrations across study cohorts

Drugs	Concentration ratios	Fold change in cohorts			
		Healthy	Outpatient	Non-ICU	ICU
Nirmatrelvir	$C_{max,plasma}:EC_{90,omicron}$	92.33	108.09	114.74	125.50
	$C_{max,plasma}:EC_{90,delta}$	30.98	36.27	38.50	42.11
	$C_{max,fluid}:EC_{90,omicron}$	31.66	35.89	37.67	40.66
	$C_{max,fluid}:EC_{90,delta}$	10.62	12.04	12.64	13.64
	$C_{max,tissue\,mass}:EC_{90,omicron}$	59.05	66.95	70.26	75.84
	$C_{max,tissue\,mass}:EC_{90,delta}$	19.82	22.47	23.58	25.45
Dexamethasone	$C_{max,plasma}:IC_{50,COVID-19}$	29.79	34.40	36.80	42.08
	$C_{max,fluid}:IC_{50,COVID-19}$	7.47	8.58	9.17	10.46
	$C_{max,tissue\,mass}:IC_{50,COVID-19}$	13.94	16.01	17.10	19.51
	$C_{max,plasma}:IC_{90,COVID-19}$	3.33	3.84	4.11	4.70
	$C_{max,fluid}:IC_{90,COVID-19}$	0.83	0.96	1.02	1.17
	$C_{max,tissue\,mass}:IC_{90,COVID-19}$	1.56	1.79	1.91	2.18
Clarithromycin	$C_{max,plasma}:MIC_{90,S.pneumoniae}$	241.33	271.20	283.40	304.15
	$C_{max,fluid}:MIC_{90,S.pneumoniae}$	138.23	153.93	160.24	174.60
	$C_{max,tissue\,mass}:MIC_{90,S.pneumoniae}$	941.04	1048.19	1091.43	1189.20
Itraconazole	$C_{max,plasma}:EC_{50,hCoV-19/Germany/FI1103201/2020}$	2.37	3.73	4.54	6.22
	$EC_{50,hCoV-19/Germany/FI1103201/2020}:C_{max,fluid}$	27.51	17.32	14.21	10.31
	$C_{max,tissue\,mass}:EC_{50,hCoV-19/Germany/FI1103201/2020}$	13.18	20.94	25.51	35.16
	$C_{max,plasma}:EC_{90,hCoV-19/Germany/FI1103201/2020}$	1.06	1.67	2.03	2.79
	$EC_{90,hCoV-19/Germany/FI1103201/2020}:C_{max,fluid}$	61.37	38.63	31.71	23.00
	$C_{max,tissue\,mass}:EC_{90,hCoV-19/Germany/FI1103201/2020}$	5.91	9.39	11.44	15.76

Figure 1
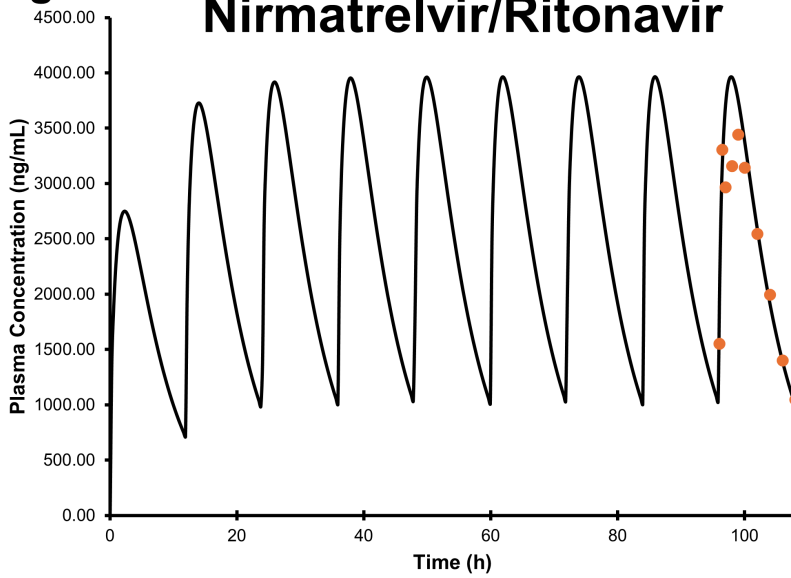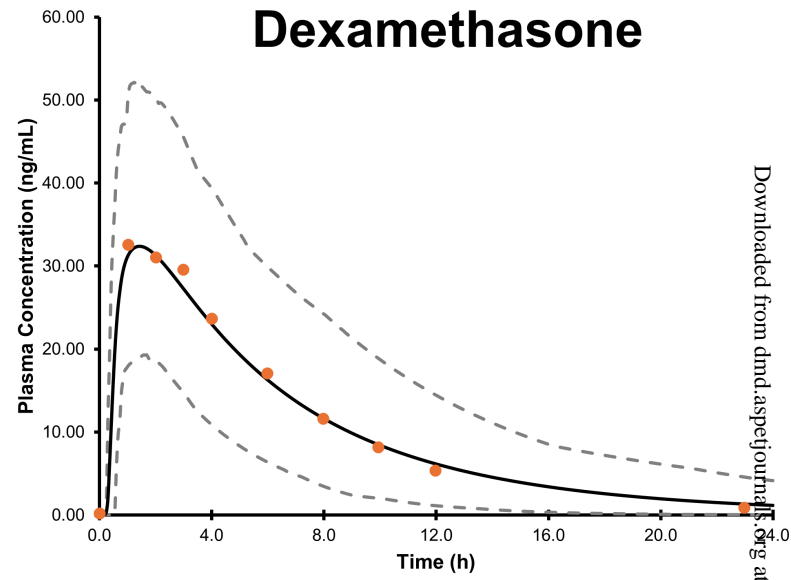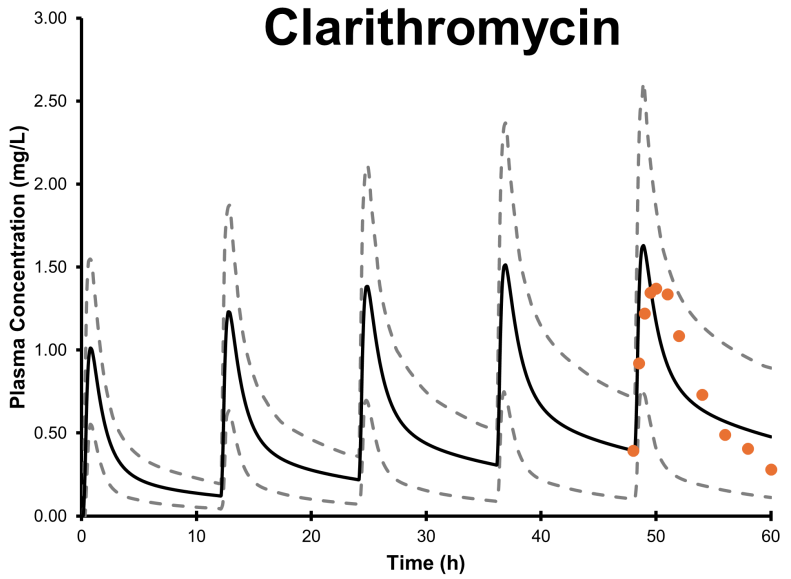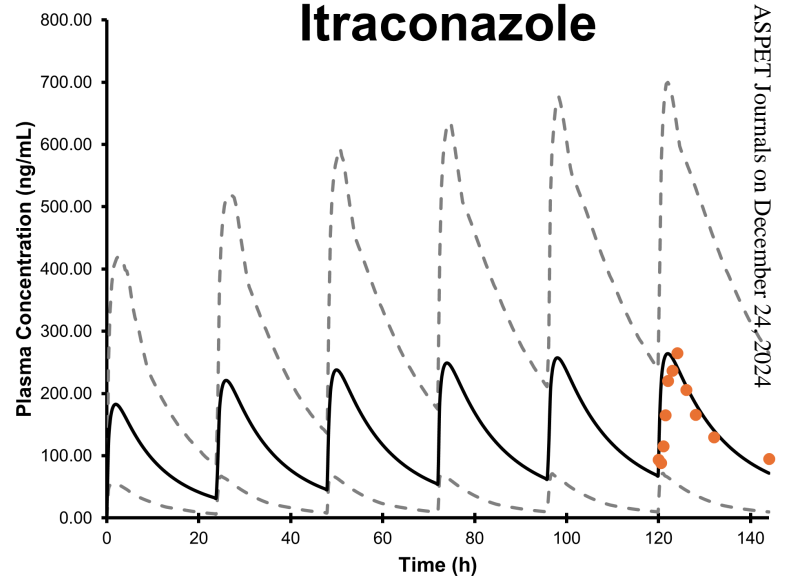
Figure 2

Nirmatrelvir/Ritonavir
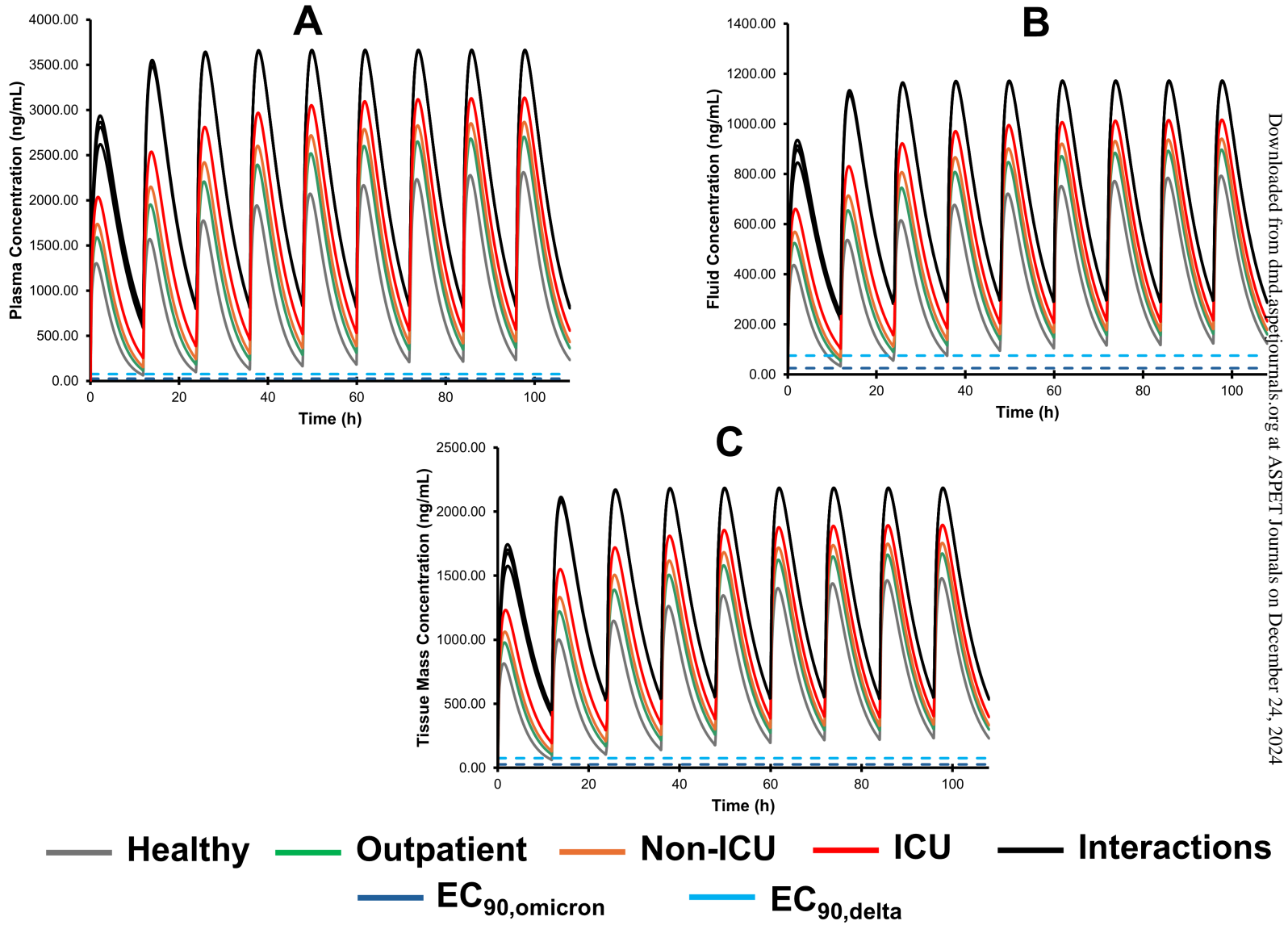
Figure 3

Dexamethasone
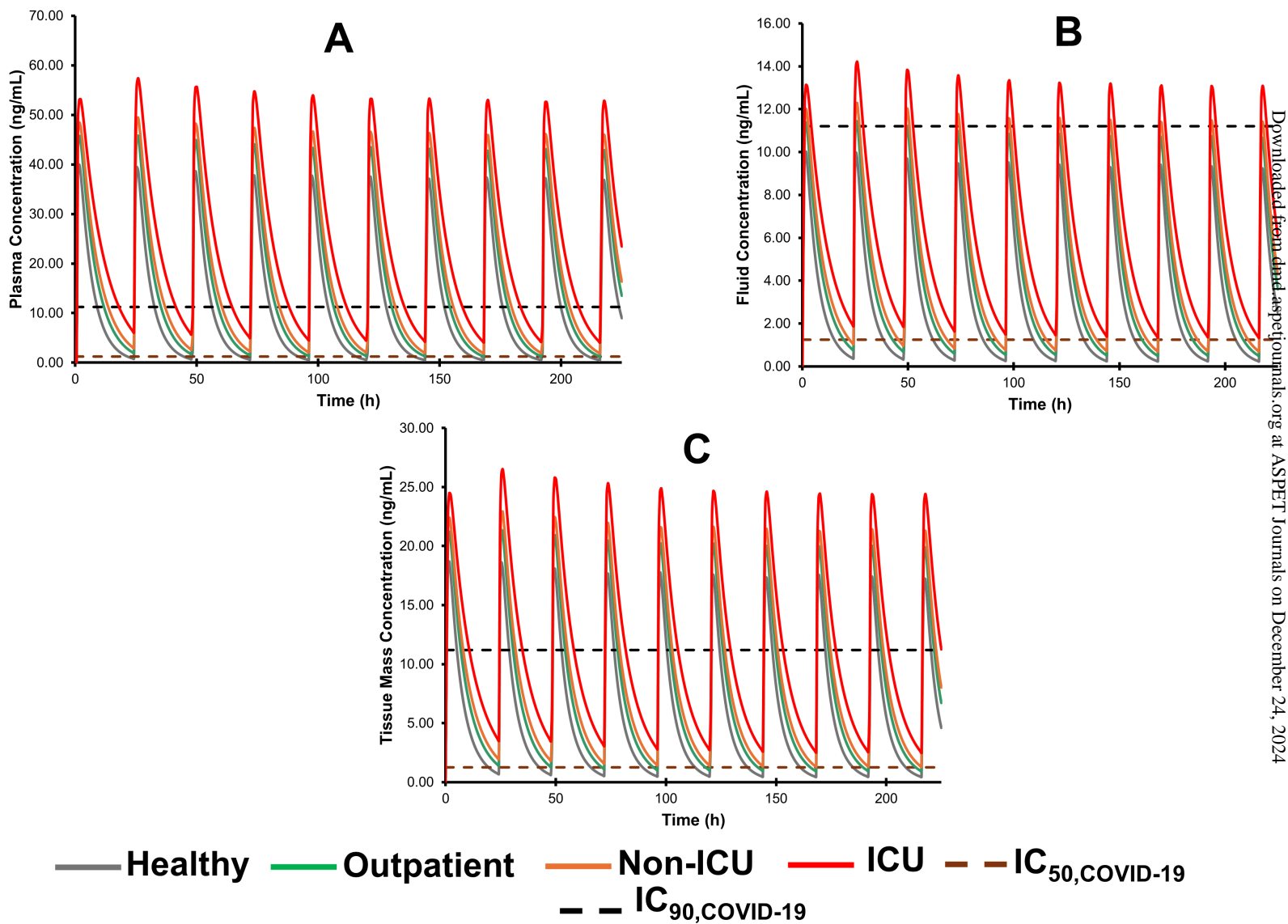
Figure 4

Clarithromycin

Figure 5

Itraconazole